Supporting Information

Near-infrared optoelectronic synapses based on a Te/α-In_2Se_3 heterojunction for neuromorphic computing

Tao YAN[1,2,5], Yuchen CAI[1,3,5], Yanrong WANG[1,3], Jia YANG[1,3], Shuhui LI[1,3], Xueying ZHAN[1,3], Fengmei WANG[1,3], Ruiqing CHENG[4], Feng WANG[1,3]*, Jun HE[4], Zhenxing WANG[1,3]*

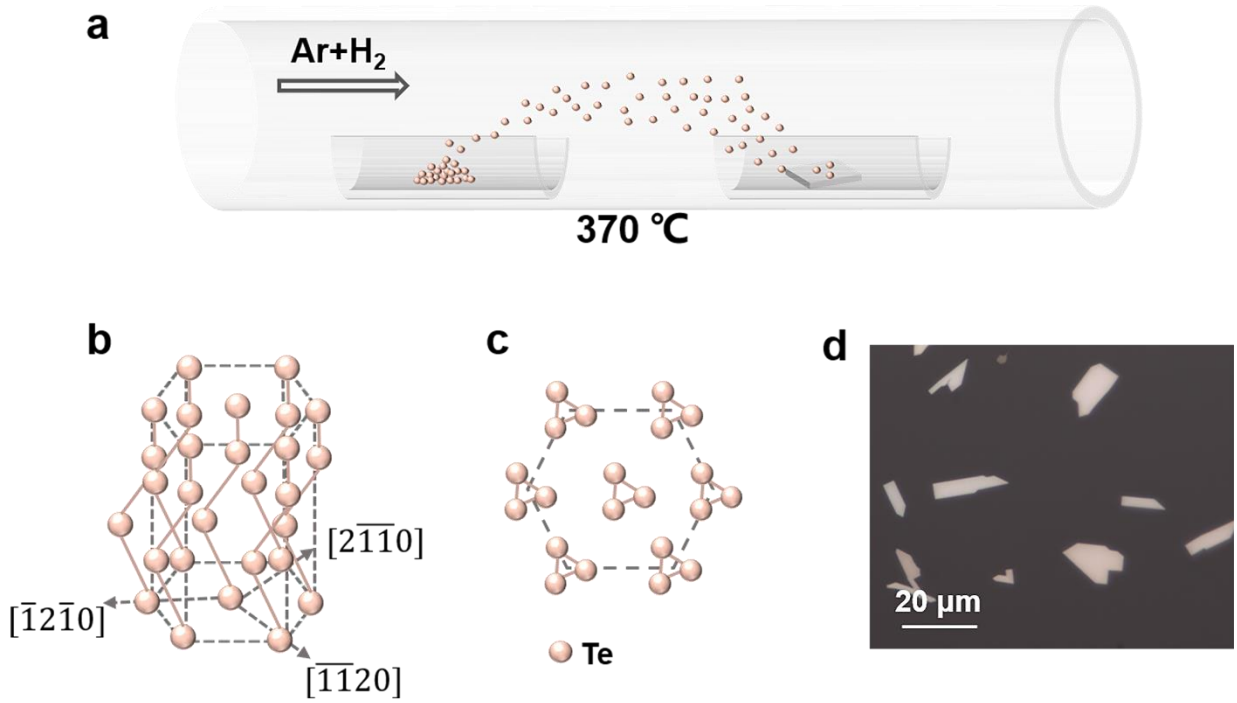

Figure S1 (a) Schematic illustration of the growth process of Te single crystals. (b) The side-view structure of Te crystal. (c) The top-view structure of Te crystal. (d) Optical microscope image of Te flakes grown on mica.

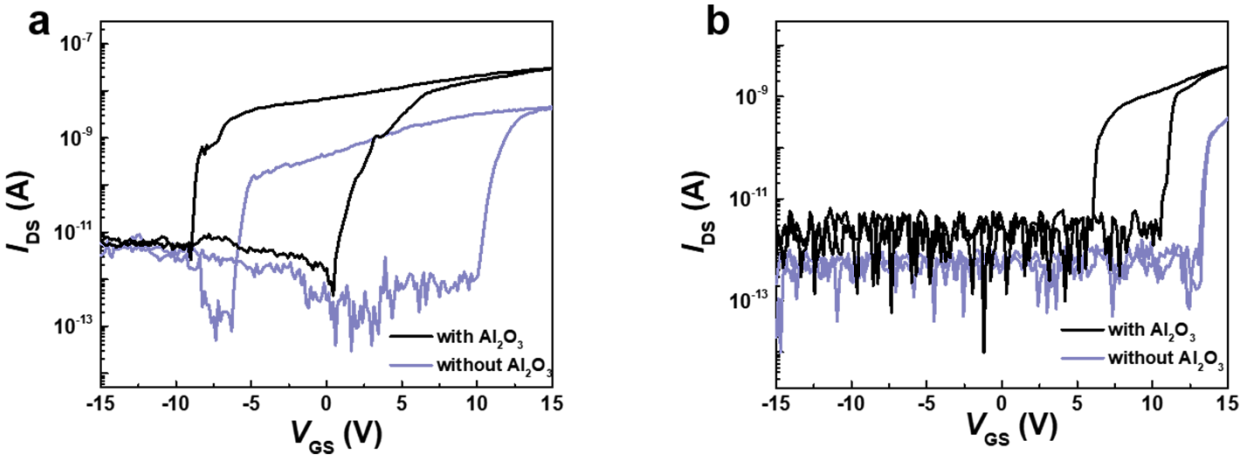

Figure S2 The transfer curves of the α-In_2Se_3 transistor with and without Al_2O_3 in 300 K (a) and 80 K(b).

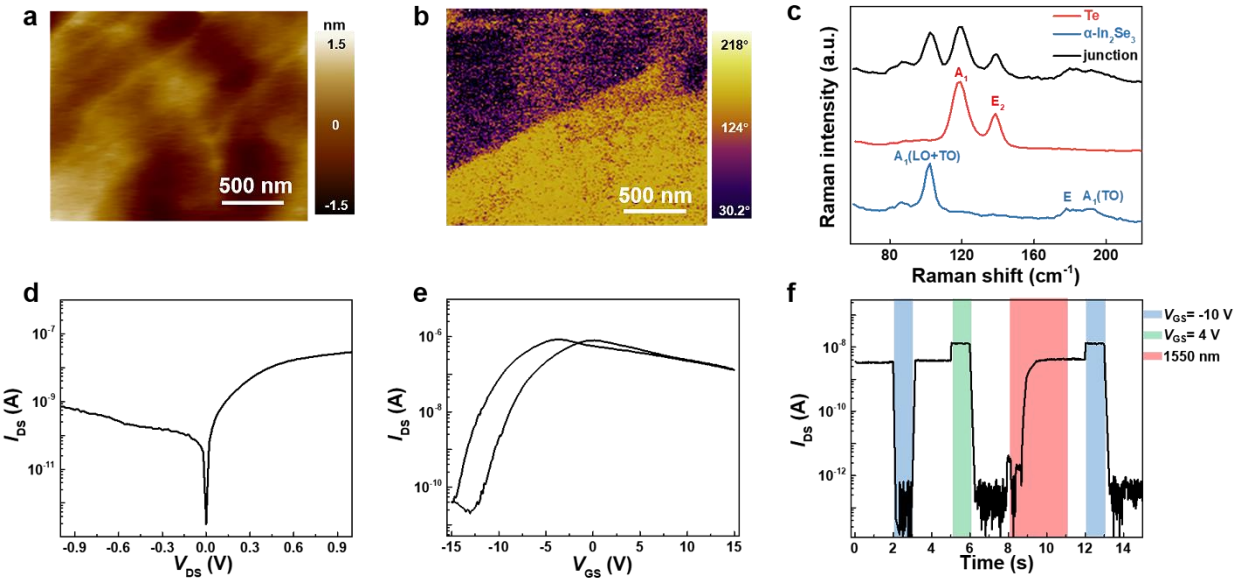

Figure S3 (a) The surface topography of an α-In_2Se_3 flake. (b) PFM phase image of the α-In_2Se_3. (c) Raman spectra of the α-In_2Se_3, Te nanosheets, and junction. (d) Output curve of the heterojunction in a dark state. (e) Transfer curve of the heterojunction in dark. (f) Response of source-drain current to different electrical pulses and a 1550 nm infrared pulse (power density = 293 mW/cm^2). Bias = 1 V.

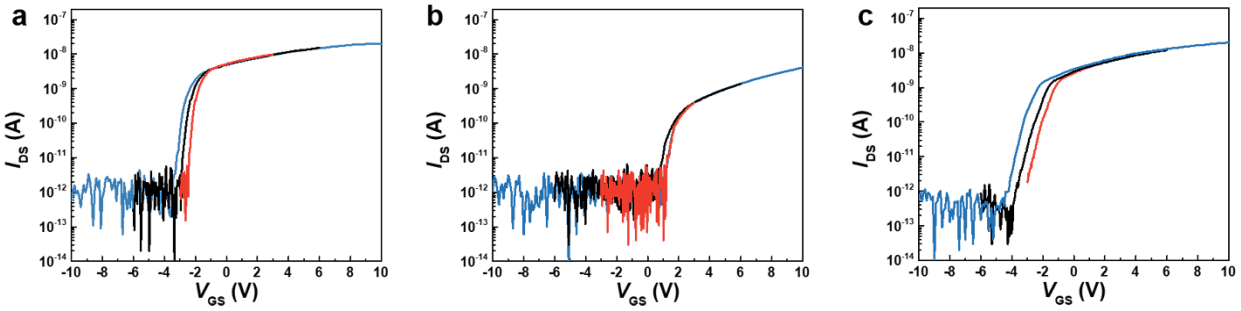

Figure S4 Transfer curves after 1550 nm pulse (a), after positive pulse (b), and after negative pulse (c), ranging from -3 V to 3 V, -6 V to 6 V and -10 V to10 V. The pulse duration is all 10 s and the amplitudes of the electrical pulses are 10 V and -10 V, respectively. Bias = 1 V.

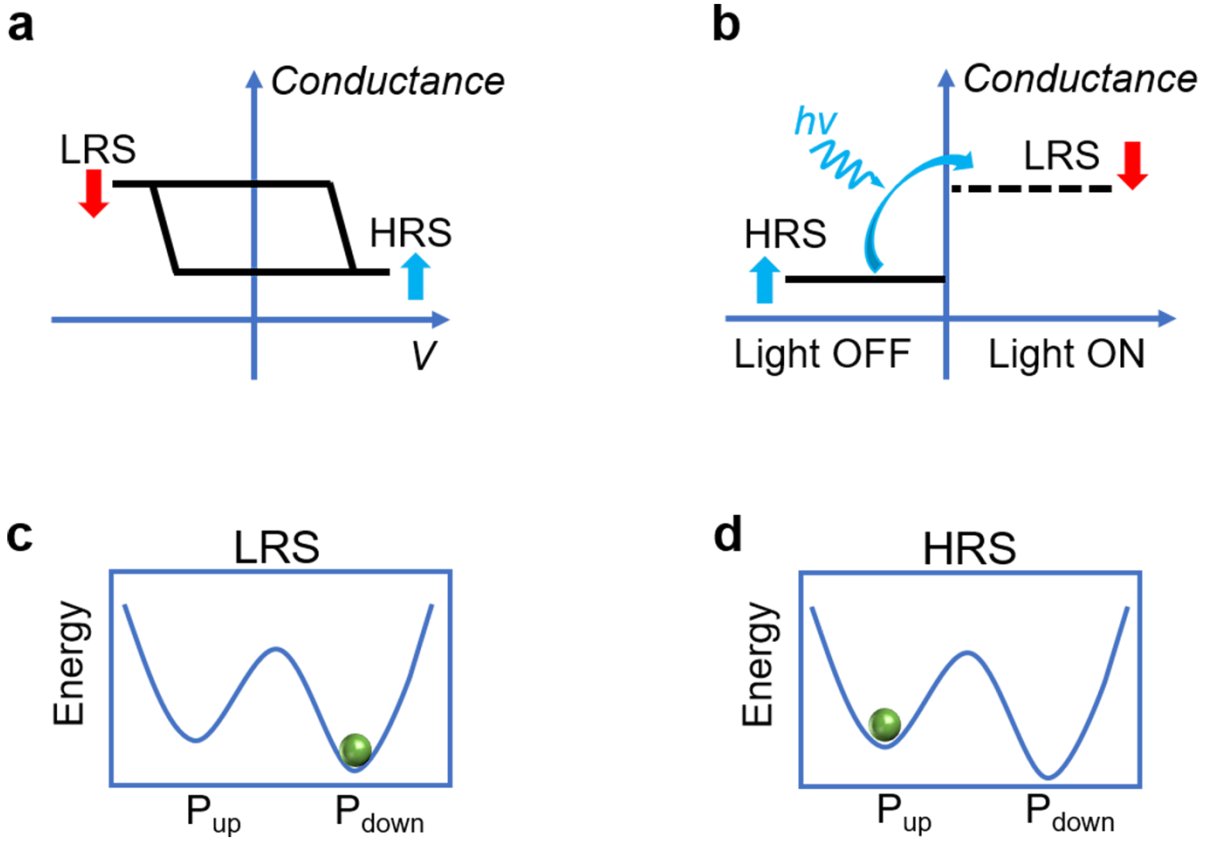

Figure S5 (a) Hysteresis curve of α-In_2Se_3 conductance with different polarization states. (b) The state of polarization upward (high resistance state) will flip to the state of polarization downward (low resistance state) under a light illumination, and the conversion is unidirectional. (c)-(d) The energy curves of different polarization states. The potential is lower when in the polarization down.

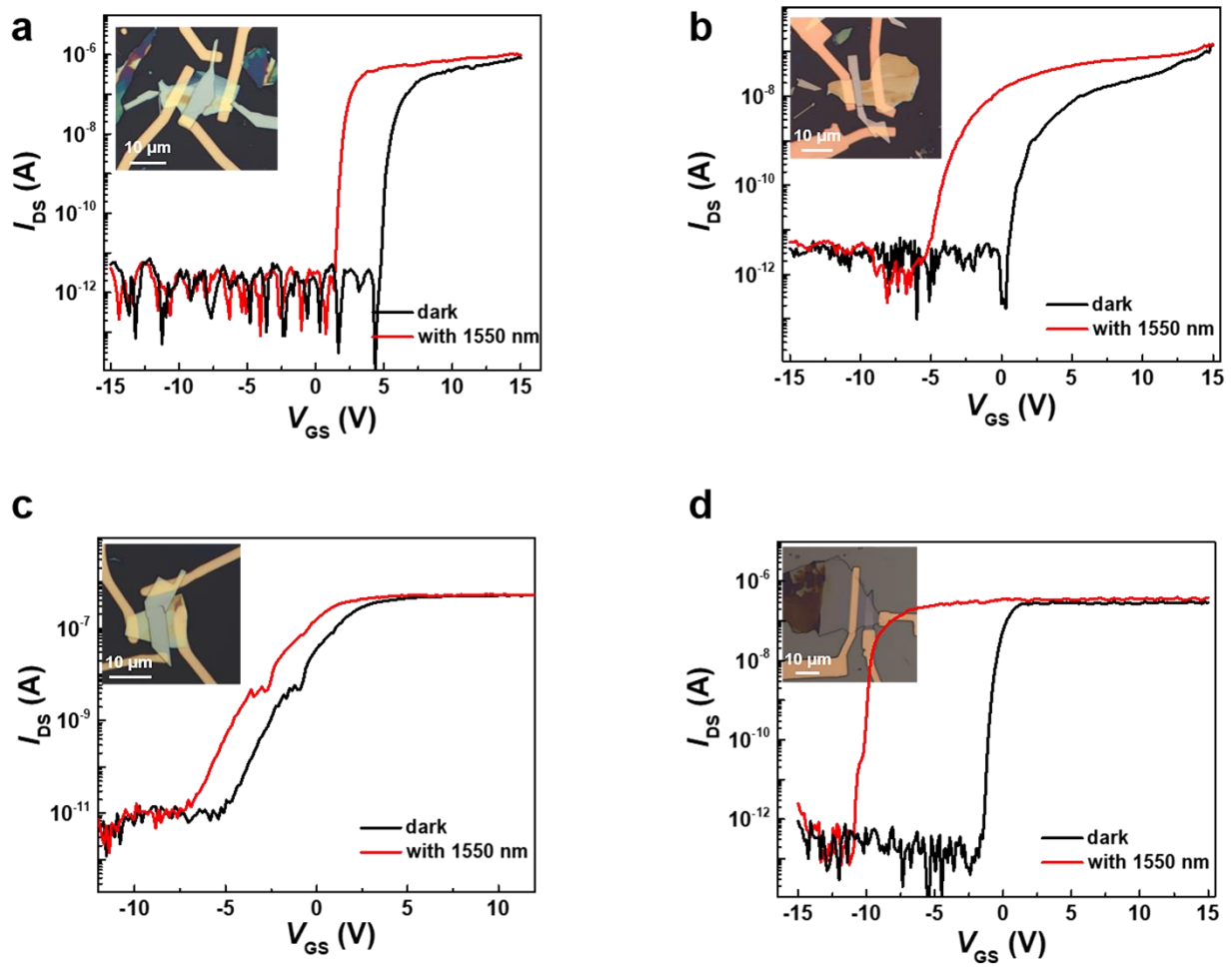

Figure S6 (a)-(d) Transfer curves of four different devices in a dark state and 1550 nm illumination. The insets show the corresponding optical microscope images of the devices.

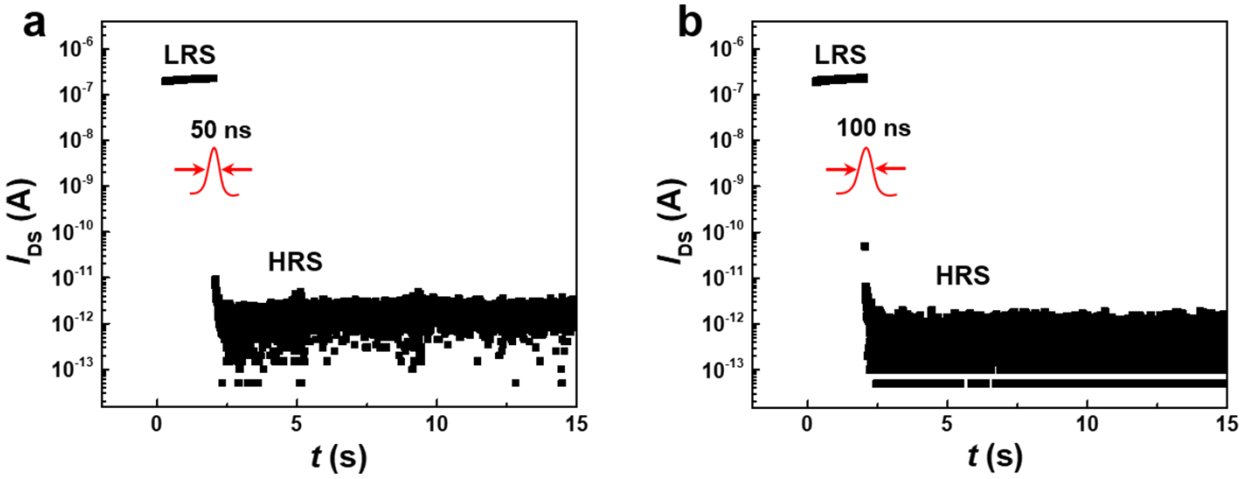

Figure S7 Time-dependent source-drain current (I_{DS}) with 50 ns electrical pulse (a) and 100 ns electrical pulse (b). The amplitude of pulse is 10 V.

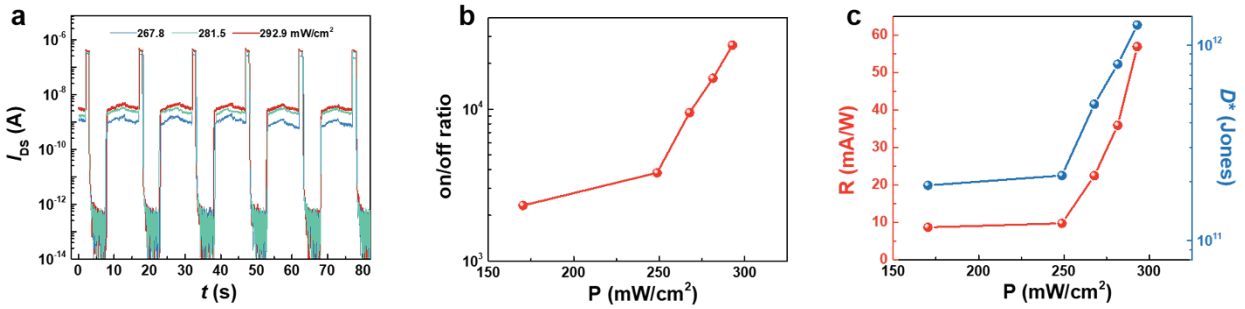

Figure S8 (a) Time-dependent source-drain current with five cycles of gate voltage (1 s) and infrared light pulses (5 s). V_{DS} = 2 V. V_{GS} = 6.5 V. (b)-(c) On-off ratio, responsibility (R) and detectivity (D*) as a function of infrared light power density. T=80 K.

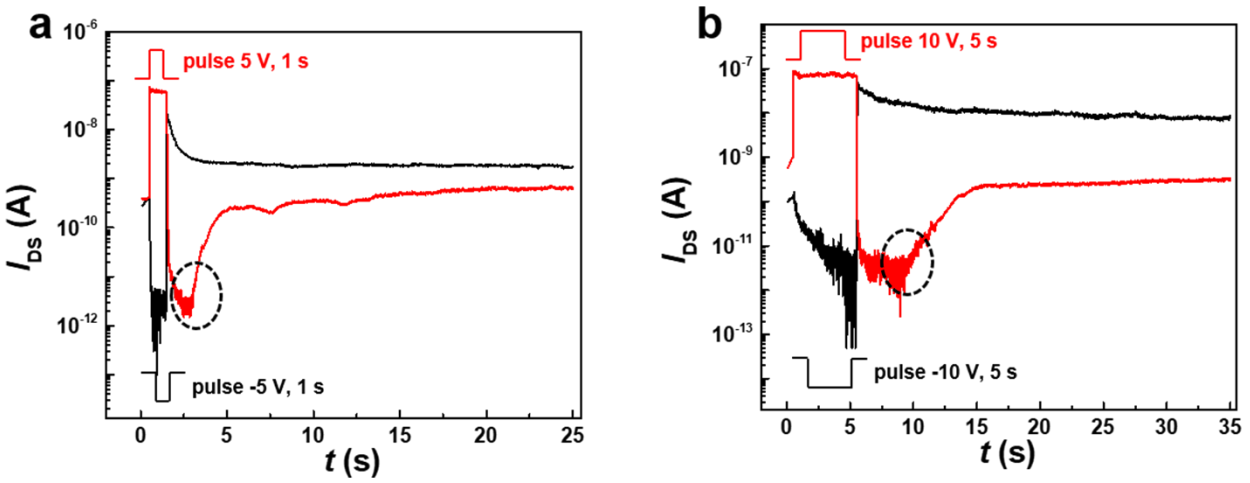

Figure S9 Time-dependent current measurement with different electrical pulses. The dashed lines mark unstable states.

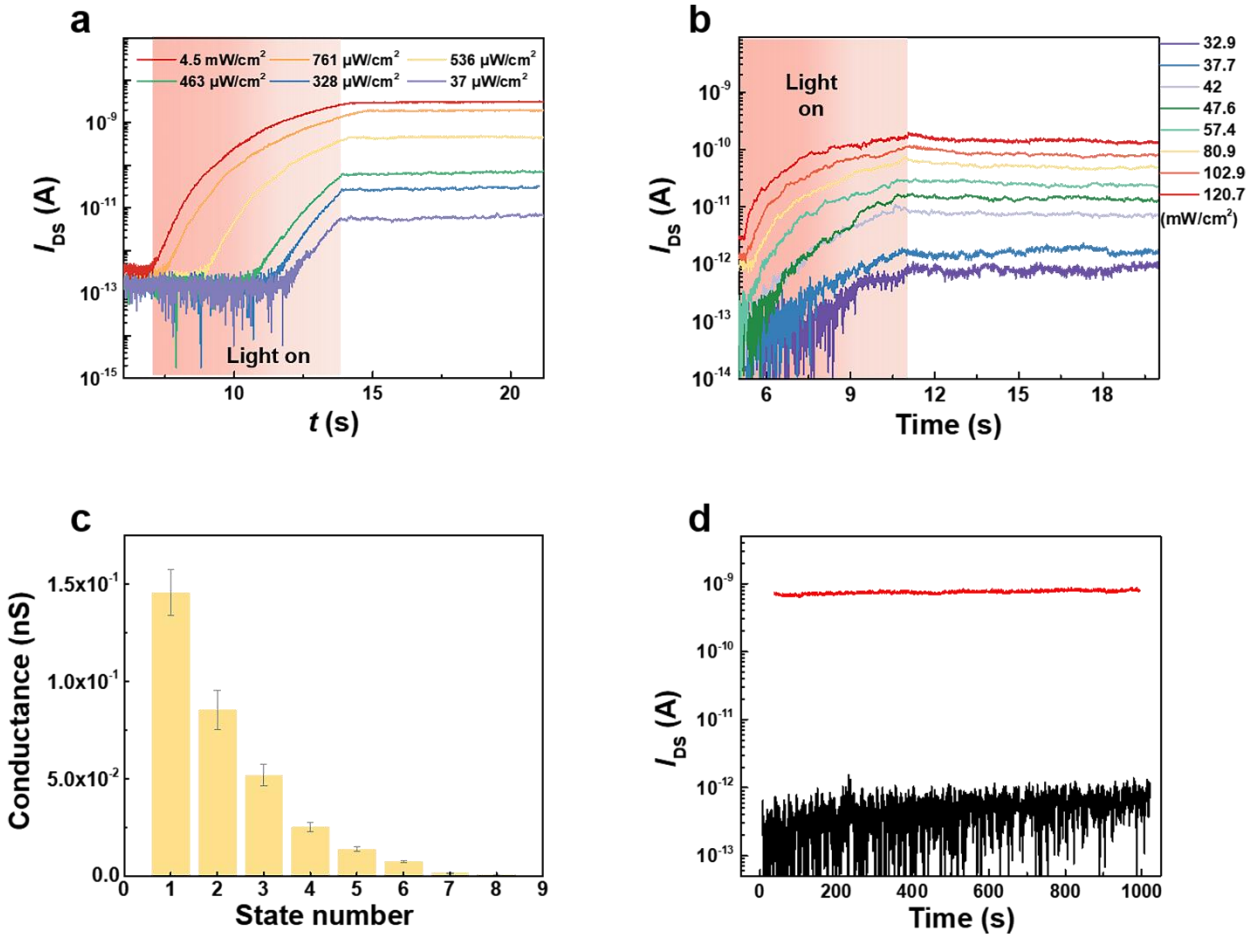

Figure S10 (a) The time-dependent source-drain current being programmed by 1550 nm illuminations with different powers densities for 7 s. (b) The time-dependent source-drain current being programmed by 1550 nm illuminations with different powers densities for 5 s. (c) The extracted 8 conductance levels after infrared pulses. (d) Retention properties of the two resistance states. V_{DS} = 1 V, T = 80 K.

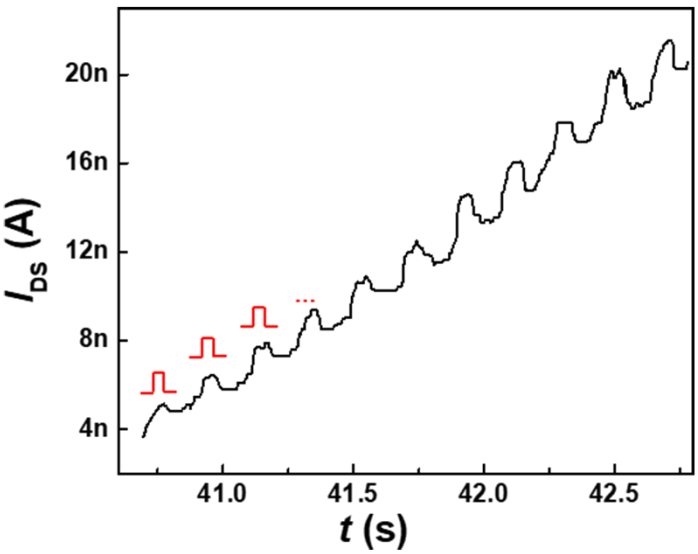

Figure S11 Time-dependent source-drain current (I_{DS}) with 1550 nm light pulses. The pulse is marked in red. The pulse width is 100 ms and the amplitude is 191 mW/cm^2.

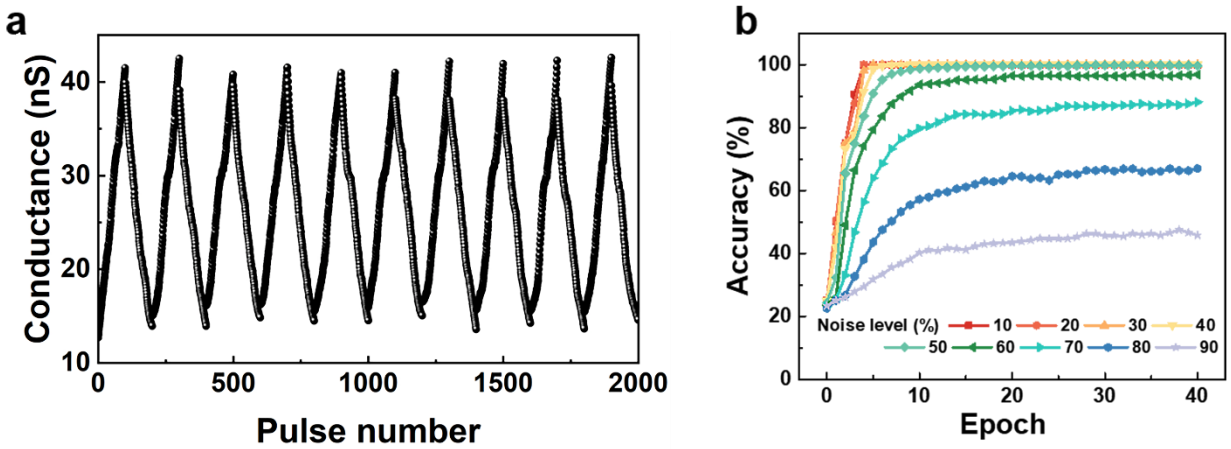

Figure R12 The device is based on a 60 nm pure α-In_2Se_3 transistor with a bottom gate of 25 nm HfO_2 and a top layer covered with 5 nm Al_2O_3. (a) The negative electrical pulse changes from -4.1 V to -5.6 V with a constant interval of 1 ms, resulting the conductance larger. The positive electrical pulse changes from 0.08 V to 0.37 V with a constant interval of 1 ms, resulting the conductance smaller. (b) Training results on pictures of letters 'NCNST' with different Gaussian noises.

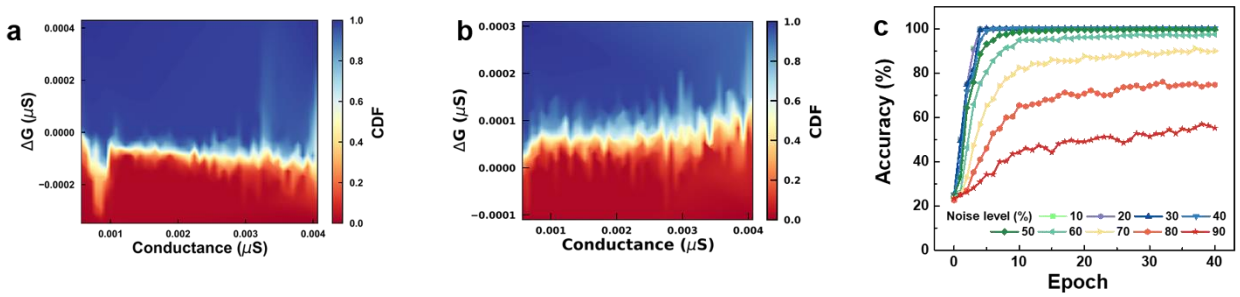

Figure S13 Heat maps of cumulative distribution function (CDF) over conductance change (ΔG) and conductance when a (a) depression (b) potentiation pulse is applied. The derivatives over ΔG tell the probability distributions at a given current conductance state. (c) The training results on inputs with different Gaussian noise.

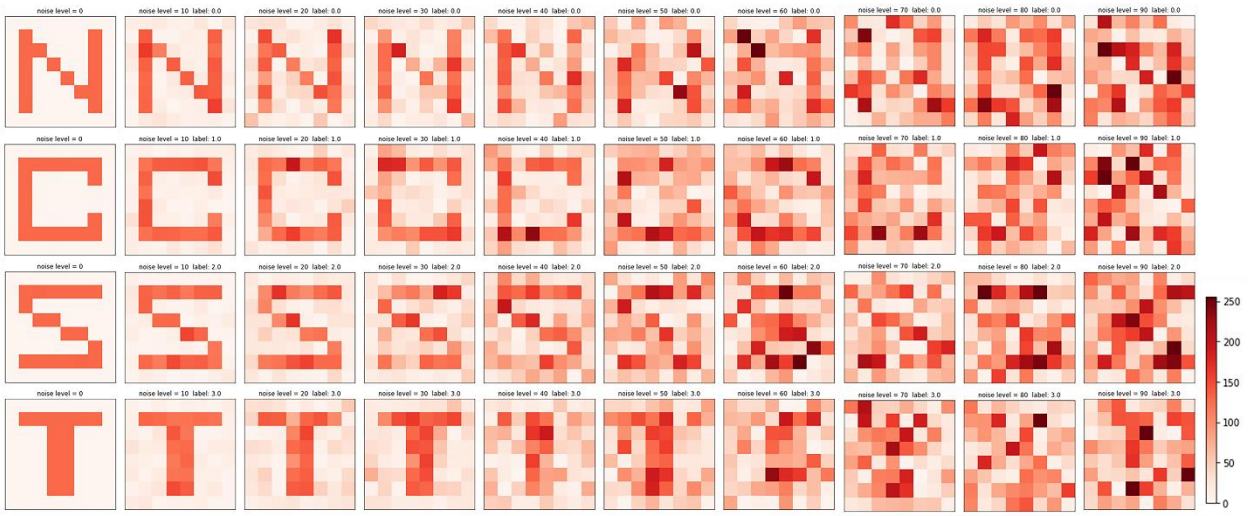

Figure S14 The pixel maps of letters "N", "C", "S", and "T" under different Gaussian noises.

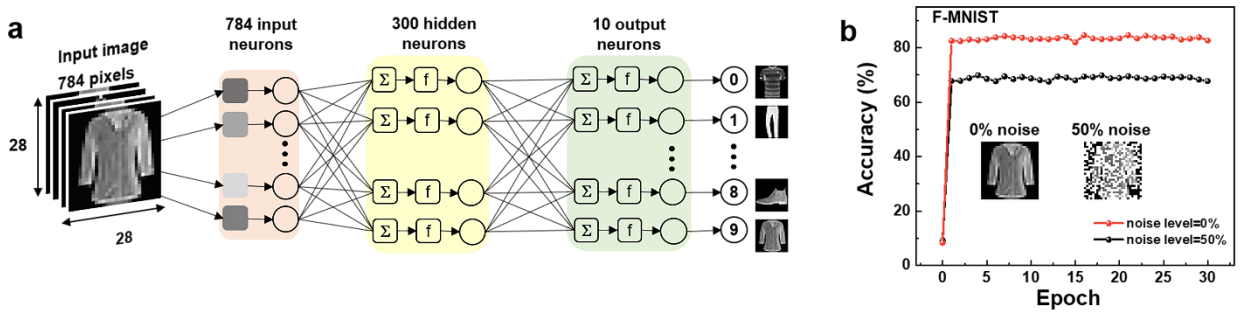

Figure S15 (a) Schematic illustration of a three-layer artificial neural network for the recognition of F-MNIST. The ANN consists of 28 × 28 input neurons, 100 hidden neurons, and 10 output neurons. (b) Training results on pictures of letters with 0% and 50% Gaussian noise. The insets show the picture when the noise is 0% and 50%. The long-term potentiation is tested by applying 1550 nm infrared pulses.

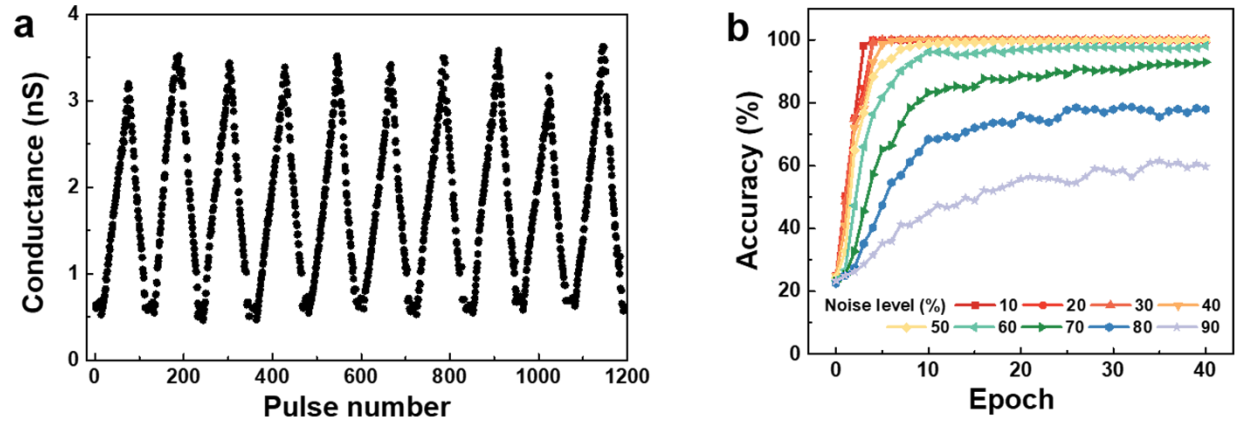

Figure S16 (a) LTP/LTD signatures of the device after applying continuous 1940 nm infrared light and electrical pulses. (b) The training results of recognition accuracy of letter images under different Gaussian noises.